J. Chem. Sci. (2021) 133:30
https://doi.org/10.1007/s12039-021-01886-6

REGULAR ARTICLE

The activation of methane by Ni-Cu/MoO_x for the synthesis of ethanol

YANNAN WANG[a], YE WANG[a,b], QING ZHAO[a], LI LI[a] and CHANGWEI HU[a,b,*]
[a]Key Laboratory of Green Chemistry and Technology, Ministry of Education, College of Chemistry, Sichuan University, Chengdu 610064, Sichuan, People's Republic of China
[b]College of Chemical Engineering, Sichuan University, Chengdu 610065, Sichuan, People's Republic of China
E-mail: changweihu@scu.edu.cn

MS received 5 September 2020; revised 7 December 2020; accepted 18 December 2020

Abstract. The conversion of methane and water to alcohols could not only reduce the greenhouse effect effectively but also improve the utilization value of methane. In the present work, Ni-Cu/MoO_x was prepared by co-impregnation method and applied to the activation of methane and water to produce ethanol. It was found that ethanol could be produced selectively mediated by Ni-Cu/MoO_x and a yield of 18.5 μmol was obtained at 240 °C, 2.5 MPa. After CH_4 cracking at 500 °C, C-O and alkoxy carbon species formed on the surface of Ni-Cu/MoO_x, while C-C coupling and the formation of $–CH_3O$ species occurred at nearly 350 °C in the cooling process. The reaction of coupled surface species with water produced ethanol, promoted by the synergetic effects of Ni, Cu and Mo active species. The direct conversion of methane to ethanol on Ni-Cu/MoO_x provided clues for the production of value-added oxygenates from methane in further study.

Keywords. methane; water; ethanol; Ni-Cu/MoO_x; cracking.

1. Introduction

Methane is not only the main component of natural gas, shale gas and natural gas hydrate, but also that of biogas and biomass pyrolysis gas, which could be considered renewable. These resources can be used directly as fuel due to the high calorific value (9510 Kcal/Nm^3) of methane.[1] Meanwhile, methane could be better used, for example, being converted to value-added products such as alcohol, aldehyde or other long-chain organics.[2,3] In general, there are two main ways for methane conversion. One is the indirect conversion, such as reforming of methane into syngas (carbon monoxide and hydrogen) at first, and then synthesizing liquid fuel, or helping synthesize other important chemical materials (such as ammonia).[4] The other is the direct conversion, such as oxidizing methane into methanol, chlorinating methane into methyl chloride, nitrifying methane into nitromethane, or converting methane to aromatic hydrocarbons.[5] Comparing with the indirect conversion, the direct conversion takes some advantages, for the reaction process is more economic and environmentally friendly, and its good prospect could be expected in the future, which attracts much attention, although there are still some shortcomings such as high energy consumption, low conversion and low selectivity.

Recently, the direct conversion of methane to alcohol has raised sustained attention because it is a good method for converting gaseous CH_4 into liquid chemicals. In this field, copper-based catalysts are usually chosen.[2,6] The activity of the previously reported copper-based catalysts for the direct conversion of methane to alcohols is displayed in Table 1, where the majority is related to methanol production, and only a few with the co-production of methanol and ethanol.

Sebastian Grundner *et al.*,[6] discovered that copper-exchanged zeolites can mimic methane monooxygenase to convert methane to methanol. Takaaki Ikuno

*For correspondence
Electronic supplementary material: The online version of this article (https://doi.org/10.1007/s12039-021-01886-6) contains supplementary material, which is available to authorized users.

Published online: 13 March 2021

Table 1. The characteristics of the catalysts for the product of alcohols from CH_4.

Catalysts	Reactants	Reaction conditions			Yield. (Me/Et)[a]	Selectivity.	Refs.
		Activation Agent and Temp.	Reaction Temp.	Pressure.			
Copper-exchanged zeolites	CH_4+H_2O	O_2 450 °C	135 °C	1 atm	160 μmol g_{cat}^{-1}(Me)	nr[b]	6
Cu-NU-1000	CH_4+H_2O	He 400 °C ,O_2 200 °C,CH_4 150 °C	135 °C	1 atm	17.7 μmol g_{cat}^{-1} (Me)	45-60%	7
Cu-SSZ-13	$CH_4+H_2O+O_2$	O_2 550 °C	210–225 °C	1 atm	0.88 ± 0.02 μmol g_{cat}^{-1} h^{-1}(Me)	70.6±0.4%	8
Cu-MOR; Si/Al = 6, 4.7 wt% Cu	CH_4+H_2O	O_2 450 °C	200 °C	36 bar	103.3 μmol g_{cat}^{-1}(Me)	nr	9,10
CuMOR(6.5)	CH_4+H_2O	Air 500 °C	200 °C	7 bar	0.204 mol mol_{Cu}^{-1}(Me)	97%	11,12
Fe/Cu–ZSM-5	$CH_4+H_2O_2$	Air 550 °C	50 °C	30.5 bar	168.4 μmol(Me)	93%	13
CeO_2/Cu_2O/Cu (111)	$CH_4+H_2O+O_2$	nr	177 °C	5.5Torr	0.9 molecules produced /10^{15} molec cm^{-2} s^{-1}(Me)	nr	14,15
Cu-0.5/PCN	$CH_4+H_2O+N_2$	photo	Room	1 atm	24.5 μmol g_{cat}^{-1} h^{-1} (Me) 106 μmol g_{cat}^{-1} h^{-1} (Et)	nr	16
Ni-Cu/MoO_x	CH_4+H_2O	CH_4 500 °C	240 °C	2.5MPa	18.5 μmol (Et)	100%	c

[a] Yield of methanol (Me) or ethanol (Et)

[b]Not reported

[c]Our present work.

et al.,[7] used copper and NU-1000 (a MOF material) to prepare Cu-NU-1000 which contained a cluster mixture of 15% Cu^{+} and 85% Cu^{2+}. In the sequential process, the catalyst sample was pretreated in O_2 at 200 °C at first, then exposed to CH_4 at 150 °C, and water was added with He flow at 135 °C, where methanol, dimethyl ether, and carbon dioxide were produced. Karthik Narsimhan *et al.,*[8] found that the mixture of methane, water and oxygen could be converted to methanol catalyzed by Cu-Na-ZSM-5 after the catalyst was calcined in O_2 at 450 °C for 5 h and exposed to CH_4 at a temperature of 200–225 °C for 0.5 h. Patrick Tomkins *et al.,*[9,10] found that with the help of O_2 activation at 450 °C for 4 h, copper-containing zeolite (Cu-MOR) could interact with methane, forming surface-bond methanol precursor, which could finally give out methanol by water extraction. Vitaly L Sushkevich *et al.,*[11,12] reported a mechanism that methane was oxidized at Cu^{2+} oxide active centres with methanol product, and water was reduced at Cu^{+} with hydrogen formation at the same time, which was proved by a series of characterization methods including *in situ* XAS, IR, and DFT calculations. Ceri Hammond *et al.,*[13] showed the conversion of methane in aqueous hydrogen peroxide catalyzed by iron- and copper-containing zeolites, and the establishment of a low-energy pathway for methane oxidation to methanol originated from the interaction between Fe-ZSM-5 and hydrogen peroxide. Zhijun Zuo *et al.*[14] and Pablo G Lustemberg *et al.,*[15] have found that only adsorbed CH_x fragments were obtained on the $CeO_2/Cu_2O/Cu$ (111) system controlled by water, which resulted in a high selectivity of methane activation to methanol. Yuanyi Zhou *et al.,*[16] reported that Cu species coordinated by PCN supplied active sites for the generation of·OH species, which enhanced photocatalytic anaerobic conversion of methane to the mixture of methanol and ethanol. From the above, it could be noticed that sometimes stronger oxidizing agents (O_2, H_2O_2, etc.) were used to help oxidize methane, or activate the catalyst sample, so that some byproducts (CO_2, CO, or DME) would be produced due to overoxidation to some extent,[6–10,17–21] which resulted in the decrease of the alcohol selectivity. Also, methane could be converted to methanol in most case, or the mixture of methanol and ethanol sometimes. Nonetheless, the synthesis of ethanol without methanol from methane have not been reported yet, which could be a brand-new research direction.

It was found previously that Ni-based catalysts could activate CH_4 at a rather low temperature,[22–24] while MoC had been reported effective for water activation.[25] Thus, in the present work, Ni-Cu/MoO_x was prepared using MoC as starting material and used for ethanol production from CH_4 and H_2O, where a yield of 18.5 μmol was obtained at 240 °C, 2.5 MPa. Meanwhile, only hydrogen was obtained from the gas product and no other types of carbon-containing byproducts emerged. With a combination of MS and XPS, it is found that $–CH_3O$ species is produced in the cracking of methane.

2. Experimental

2.1 *Sample preparation*

The Ni-Cu/MoO_x sample was prepared by the co-impregnation method. 0.4954 g of $Ni(NO_3)_2{\cdot}6H_2O$ (Keshi, ≥98%) and 0.0624 g of $Cu(CH_3CO_2)_2{\cdot}H_2O$ (Guangfu Fine Chemical, 99.0%) were dissolved in 10 mL water. 2.000 g of MoC (Strem Chemicals, Inc. 99.5%-Mo) was impregnated with the above-mentioned solution for 24 h under ambient condition. Afterwards, the sample was dried at 85 °C for 1.5 h and then at 110 °C for 4 h. The obtained sample was ground into a powder and then calcined at 500 °C (with a ramp rate of 2 °C/min) in a muffle furnace (XMT-6000AS) for 5 h under air atmosphere. Finally, the Ni-Cu/MoO_x was gained. For comparison, the MoO_x, Ni/MoO_x, and Cu/MoO_x were prepared by the same method above using pure water (to eliminate the effect of water on the variation of composition and structure of the samples), $Ni(NO_3)_2$ solution, and $Cu(CH_3CO_2)_2$ solution, respectively for impregnation of MoC.

Before the activity test, a pretreatment was carried out in a fix-bed tubular quartz microreactor for Ni-Cu/MoO_x: the obtained 0.25 g sample was reduced at 500 °C for 1 h with $F(Ar) = F(H_2) = 30$ mL/min (Cheng Du Tai Yu Gas Co., Ltd.), and then CH_4 cracking was carried out at 500 °C for 1 h with $F(CH_4) = 30$ mL/min (Cheng Du Tai Yu Gas Co. Ltd.). Then the system was cooled down to room temperature in CH_4 flow.

2.2 *Activity test*

Next, the thus-obtained sample was transferred into a 50 mL stainless autoclave reactor (Beijing Century Senlong experimental apparatus Co., LTD.) for the activity tests with 20 mL deionized water introduced. At last, methane was filled into the autoclave until 2.5 MPa, and the reaction was conducted at 240 °C for 4 h. During the reaction, the pressure could attain nearly 7.5 MPa, and the water was in liquid phase. After the reaction, the gas collected from the autoclave

was analyzed by a gas chromatograph equipped with the AT PLOT C-2000 capillary column (Kexiao Instrument, China) and thermal conductivity detector (Figure S1, Supplementary Information), and the liquid product was analyzed by a gas chromatograph equipped with a DB-624 capillary column (Agilent) and flame ionization detector. (Figure S2, Supplementary Information). Simultaneously, for comparison, the gas chromatogram of a standard sample for methanol, ethanol, and internal standard substance was also obtained and shown in Figure S3, Supplementary Information. The calculation using an internal standard method was shown as the followings:

$$m_e = f \times \frac{m_s A_e}{A_s} (1) \quad (1)$$

$$Y_e = \frac{m_e}{M_e V} (2) \quad (2)$$

where m_e, m_s were the mass of ethanol product and internal standard (2-propanol), A_e, A_s were the peak area of ethanol product and internal standard, and f was the relative correction factor of ethanol to an internal standard. Y_e was the yield of ethanol product, M_e was the molar mass of ethanol, and V was the total volume of the liquid product.

2.3 *Characterization*

The XPS experiments were performed on an AXIS Ultra DLD (KRATOS) spectrometer with the Catalytic Chamber using monochromated Al radiation. The data were referenced using the C 1s peak at the binding energy of 284.6 eV. Before the experiments, the sample was reduced at 500 °C in H_2/Ar for 1 h, and then CH_4 was cracked at 500 °C for 1 h. The sample was cooled down to room temperature under CH_4 atmosphere after cracking. For comparison, another sample reduced at 500 °C in H_2/Ar for 1 h and then cooled down to room temperature under H_2/Ar atmosphere without cracking was also prepared. After the treatment, the sample was transferred into the XPS Vacuum Chamber in a glovebox to avoid exposure to air (thus the only contamination could be water formed in the reduction), and the spectra were recorded at room temperature afterwards.

The *in situ* Diffuse Reflectance Infrared Fourier Transform Spectroscopy (*in situ* DRIFTS) experiments were operated on the Bruker Infrared Spectrometer (FT-IR V70). The sample was reduced at 500 °C in H_2/Ar for 1 h and then cooled down to room temperature in Ar atmosphere, and the background of every scanned temperature was obtained with MCT detector (resolution 4 cm^{-1}) during the cooling time simultaneously. Prior to the experiments, the dilute feed gas with the flow rates $F(CH_4)$ = 4 mL/min and $F(Ar)$ = 16 mL/min flowed for 1 h at room temperature, and then the *in situ* DRIFTS CH_4 temperature-programmed decomposition (TPDe) experiment was carried out in the above feed gas with the sample heated from room temperature to 500 °C with the rate of 10 °C/min.

The Mass Spectrum experiments were carried out using on-line multichannel HPR-20QIC mass spectrometry. The effluent from CH_4 cracking on Ni-Cu/MoO_x was analyzed with the flow rates $F(CH_4)$ = 30 mL/min. And the signal of m/z from 1 to 200 could be detected.

The Raman Spectra experiments were performed on a HORIBA R-XploRA Plus instrument with the excitation wavelength of 638 nm. The wavenumber values of Raman shift were measured in the range of 300−3000 cm^{-1} with three scans on average.

3. Results and Discussion

3.1 *Activity results*

The activity results in the liquid-solid dynamic condition over MoO_x, Ni/MoO_x, Cu/MoO_x and Ni-Cu/MoO_x samples are shown in Table 2. It is obvious that MoO_x shows no activity, and Ni/MoO_x and Cu/MoO_x show moderate activity with an ethanol yield of 3.0 and 0.9 μmol, respectively. Interestingly, Ni-Cu/MoO_x could give the highest EtOH yield of 18.5 μmol. These results point out the importance of the co-existence of nickel and copper for enhancing the EtOH yield.

Considering the fact that the pretreatment is also vital, the activity tests of Ni-Cu/MoO_x were carried out via different pretreatments, and the results were shown in Table 3. It was obviously noticed that no activity was shown in the blank experiment without pretreatment. If the cracking was carried out without reduction, no activity would be observed, and the same was true when only reduction was carried out with no subsequent CH_4 cracking. Therefore, the above data indicate that both the reduction and cracking processes are important steps for obtaining ethanol by the action of Ni-Cu/MoO_x. Furthermore, the cracking temperature is also important, only a low yield of ethanol (3.7 μmol) was observed when the cracking temperature was 300 °C. While the cracking was carried out at 500 °C, much higher activity was observed. Comparing with the results in the literature (Table 1), a distinct

Table 2. The activity of different samples under the same pretreatment conditions.

Samples	EtOH Yield (μmol)
MoO_x	0
Ni/MoO_x	3.0
Cu/MoO_x	0.9
$Ni\text{-}Cu\ /MoO_x$	18.5

Pretreatment conditions: 0.25 g of the sample was reduced at 500 °C for 1 h with $F(Ar) = F(H_2) = 30$ mL/min, and then CH_4 cracking was carried out at 500 °C for 1 h with $F(CH_4) = 30$ mL/min.

Table 3. The activity of $Ni\text{-}Cu/MoO_x$ sample under the different pretreatment conditions.

Pretreatments	EtOH Yield (μmol)
No pretreatment	0
Reduction at 500 °C without cracking	0
Cracking at 500 °C without reduction	0
Reduction at 500 °C and cracking at 300 °C	3.7
Reduction at 500 °C and cracking at 500 °C	18.5

Other same conditions: 0.25 g of the sample was reduced for 1 h with $F(Ar) = F(H_2) = 30$ mL/min, and CH_4 cracking was carried out for 1 h with $F(CH_4) = 30$ mL/min.

advantage could be noticed that methane and water were converted to ethanol by the mediation of $Ni\text{-}Cu/MoO_x$, and no other carbon-containing byproducts were produced. A couple of experiments at different reaction time were performed and the results were shown in Table S1, Supplementary Information. It was obvious that 4 h was the best reaction time for the experiment.

3.2 *XPS*

As shown in Figure 1, it could be noticed that the peaks at binding energy of 285.8 and 287.1 eV appeared after reduction besides that of 284.6 eV, because the MoC has not been converted to MoO_x during the preparation process, while the binding energy of nearly 530.3 eV corresponded to the oxygen ions of the crystal lattice(O^{2-}). [26,27] In addition, the intensity of the peak at 532.2 eV was very strong. Kim J H *et al.* and Qiu *et al.*,[28,29] supposed that the binding energy of 532.4 eV was attributed to adsorbed water, while Liu Y *et al.*,[30] suggested that the peaks at 532.1 eV were per the characteristics of MoO_2. Comparing with the results in literature and the present work, the binding energy of 532.2 eV might be the overlapped peak of chemisorbed water from the reduction of the $Ni\text{-}Cu/MoO_x$ and the species related to Mo. For metal species, it could be seen that the peaks at the binding energy of 932.0 and 934.5 eV emerged in Cu 2p XPS results. According to the literature, the peak at 934.5 eV corresponded to Cu^{2+} species, and that at 932.0 eV was attributed to Cu^{+} species when confirmed by Cu-Auger results of $Ni\text{-}Cu/MoO_x$ in Figure 2.[31–34] The peaks at the binding energy of 229.4 and 232.5, 231.1 and 234.1, and 232.6 and 235.7 eV corresponded to Mo^{4+}, Mo^{5+}, and Mo^{6+}, respectively.[35–37] It could be noticed that Mo^{6+} species showed relatively low intensity. Although Ni oxides could be reduced to metal at 400 °C reported in the literature,[37] in the Ni 2p XPS results (Fig. 1e), only Ni^{2+} (856.1 eV) species could be detected,[38] which demonstrated the strong interactions between Ni^{2+} species with Cu or Mo species and might be caused by the relatively short reduction time (1 h) and the formation of a special environment combined with Ni, Cu and Mo in the sample under the present conditions, or the contamination of water from the reduction, since the sample was protected before XPS measurement, which deserves further investigation.

When the sample was cooled in CH_4 atmosphere after cracking at 500 °C, the intensities of peaks at the binding energy of 285.8 and 287.1 eV increased a lot. Meanwhile, the Ni-C (281.5 eV) species could be noticed,[39] and the peak at the binding energy of 288.7 eV also appeared in the C 1s XPS results. Wang Z *et al.*,[40] suggested that the binding energy of 285.6 eV were attributed to sp^3C species. Cui Y et al. and Schuster M E *et al.*,[41,42] considered that the binding energy near 286.0 eV was the peak of C-O-H or C-O-C species. Zhang LB *et al.* and Kim H J *et al.*,[43,44] assumed that the binding energy of 287.1 eV was ascribed to epoxy carbon, C-O or C=O species, respectively. Óvári L *et al.*,[45] suggested that the binding energy of 288.7 eV corresponded to alkoxy carbon species from ethanol, while Shankhamala Kundu *et al.*,[46] considered that those species were corresponding to -COO species. By comparison of these literature results with that in the present work, the binding energy of 285.8 eV could be attributed to C-O species. Considering the characteristic of the present system, the binding energy of 287.1 eV was assigned to another type of C-O species, and that of 288.7 eV was assigned to alkoxy carbon species which were the essential precursor of ethanol synthesis. Meanwhile, an obvious decrease of the intensity of the peak at 532.2 eV could be noticed, which was caused by the conversion of Mo=O species to O-Mo-O species, while -OH bond species (531.2 eV)

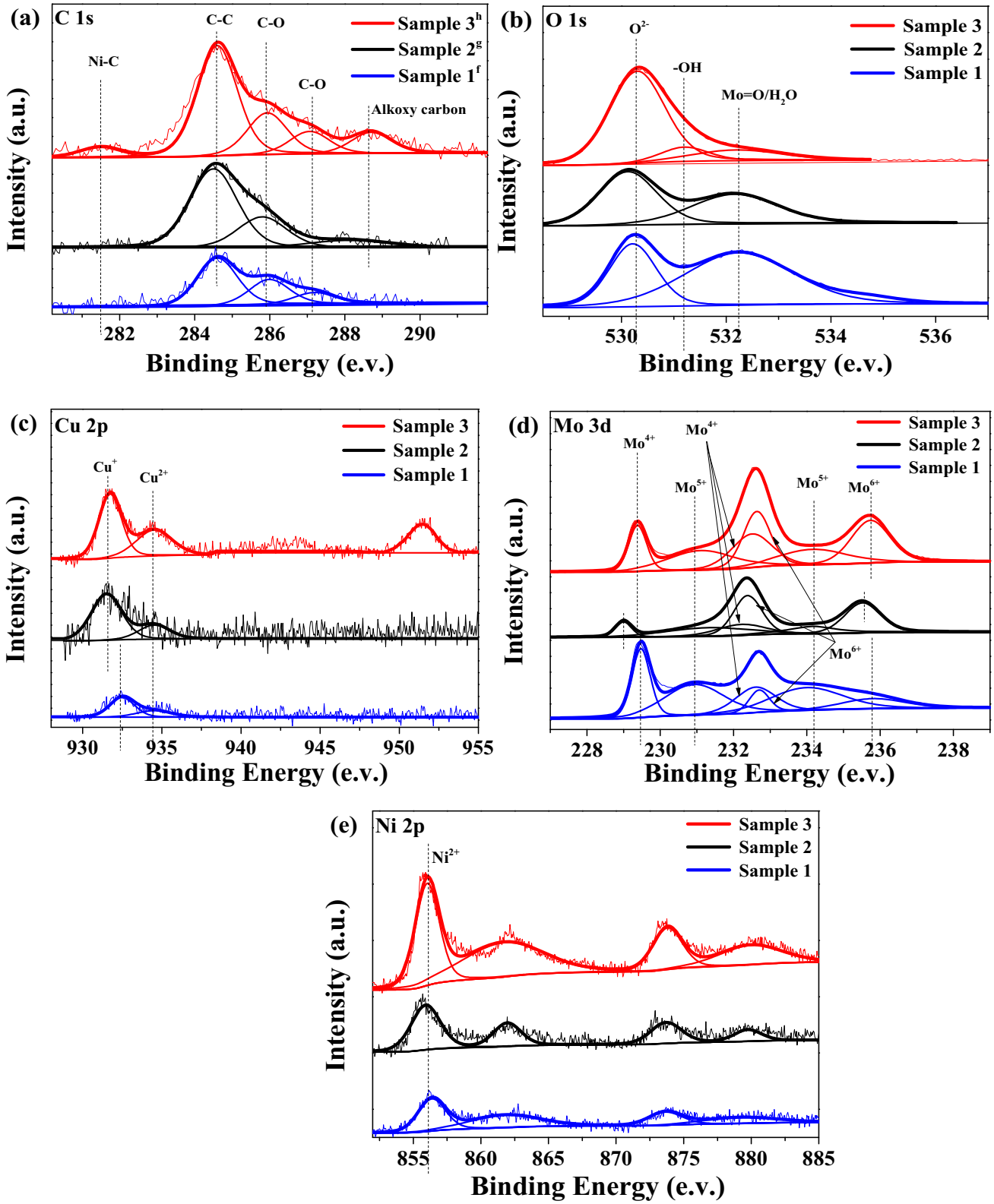

Figure 1. XPS results of Ni-Cu/MoO_x samples: (**a**) C 1s, (**b**) O 1s, (**c**) Cu 2p, (**d**) Mo 3d, (**e**) Ni 2p. (**f**) Sample 1: the Ni-Cu/MoO_x was cooled in H_2 atmosphere after reduction and before cracking. (**g**) Sample 2: the Ni-Cu/MoO_x was cooled in Ar atmosphere after cracking. (**h**) Sample 3: the Ni-Cu/MoO_x was cooled in CH_4 atmosphere after cracking.

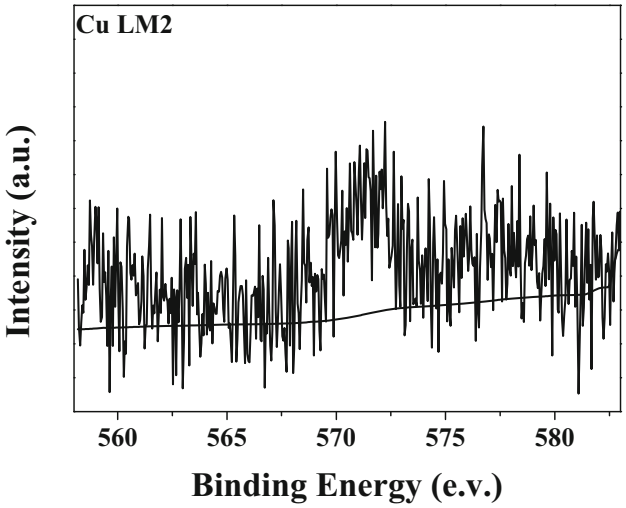

Figure 2. Cu-Auger spectrum result of Ni-Cu/MoO_x samples.

with weak intensity emerged in the O 1s XPS results.[47] Therefore, it could be deduced that there was also an interaction between the hydrogen from CH_4 cracking and the oxygen on the surface of Ni-Cu/MoO_x,[28] which might help the formation of alkoxy and -OH species. For metal species, as shown in Table 4, it was seen that the content of Cu species showed a decrease for Cu^{2+} (from 45% to 39%), and an increase for Cu^{+} (from 55% to 61%) was observed after cracking. Meanwhile, it could be also distinguished that a decrease content of Mo^{5+} (from 51% to 31%) and increased content of Mo^{6+}(from 16% to 41%) and Mo^{4+}emerged (from 33% to 28%), while Ni^{2+} kept stable relatively. Herein, some Cu^{2+} and Mo^{5+} species were converted to Cu^{+} and Mo^{6+} species, respectively, which suggested that both Cu and Mo supplied electrons to combine with H_{ads} or $CH_{3,ads}$ from CH_4 cracking on the surface of Ni-Cu/MoO_x. When the sample was cooled in Ar atmosphere after cracking, the peak of C-O species vanished, and alkoxy carbon almost disappeared. Compared with the sample before cracking, the intensity of Mo-O and Cu^{2+} species was in the downtrend, while the intensity of Cu^{+} and Mo^{6+} was in the uptrend. It could be observed that the variation of metal was similar with that when Ni-Cu/MoO_x sample was cooled in CH_4 atmosphere after cracking. However, the C-O species vanished and -OH was not emerged in Ar atmosphere. Therefore, the phenomenon further indicated that the co-operation of Ni, Mo and Cu sites and CH_4 atmosphere could keep the adsorbed species when the temperature was below 500 °C, which could play an important role in the conversion of methane to ethanol.

3.3 *In situ DRIFTS*

The *in situ* DRIFTS experiment was performed and the result of CH_4 temperature-programmed cracking on Ni-Cu/MoO_x sample was shown in Figure 3. The IR band at 1270 and 1304 cm^{-1} corresponded to the peaks of gaseous methane.[22,23] The IR band at 1354 cm^{-1} was the characteristic of asymmetric deformation vibrations of adsorbed CH_3 species.[48,49] The IR band at 1033 cm^{-1} was assigned to –OH bending species.[50] The emergence of IR band at 1333 cm^{-1} was attributed to C-O species, [51] and the large intensity of IR band at 1342 cm^{-1} could be noticed at low temperature. According to the literature,[23] a small peak at 1342 cm^{-1} was found for the adsorption of CH_4 *via in situ* DRIFTS on Ni-Si/ZrO_2. Qiushi Pan *et al.,*[52] suggested that the IR band at 1340 cm^{-1} could be assigned to C-H vibration of -CH_2, and especially it could be part of -CH_2OH species which might be a further precursor of formate hydrogenation. J. C. Lavalley *et al.,*[53] thought that the band at 1550, 1440, 1345 cm^{-1} was ascribed to acetate species which might be an intermediate for CO hydrogenation to alcohol. By comparison of these literature results with that in the present work, it could be proposed that the IR band at 1342 cm^{-1} obtained in the cracking and cooling process could be assigned to a kind of special precursor of ethanol synthesis, which was caused by the interaction between cracked CH_4 and Ni-Cu/MoO_x. CH_4 could be cracked to CH_3 species on Ni species at first, and the cracked CH_3 species could migrate to Cu or Mo atom and be converted to another species by the co-operation of Ni, Cu, Mo and O species, especially when the temperature was below 400 °C. Therefore, the cracking process was necessary and the temperature of subsequent reaction with water could not be too high.

3.4 *Mass spectrum*

To trace the precursor variation, the online mass spectrum of the effluent from the Ni-Cu/MoO_x sample on the whole cracking process was recorded and shown in Figure 4. Considering the events that happened at different time points, "t_1", "t_2", "t_3" and "t_4" were used to describe them for more convenience. The condition before t_1 was reduction period of the sample and at t_1 the mixture flow of H_2 and Ar was switched to CH_4 for cracking. When CH_4 was started to flow in the system, the cracking process started (t_1), which caused the fluctuation of the

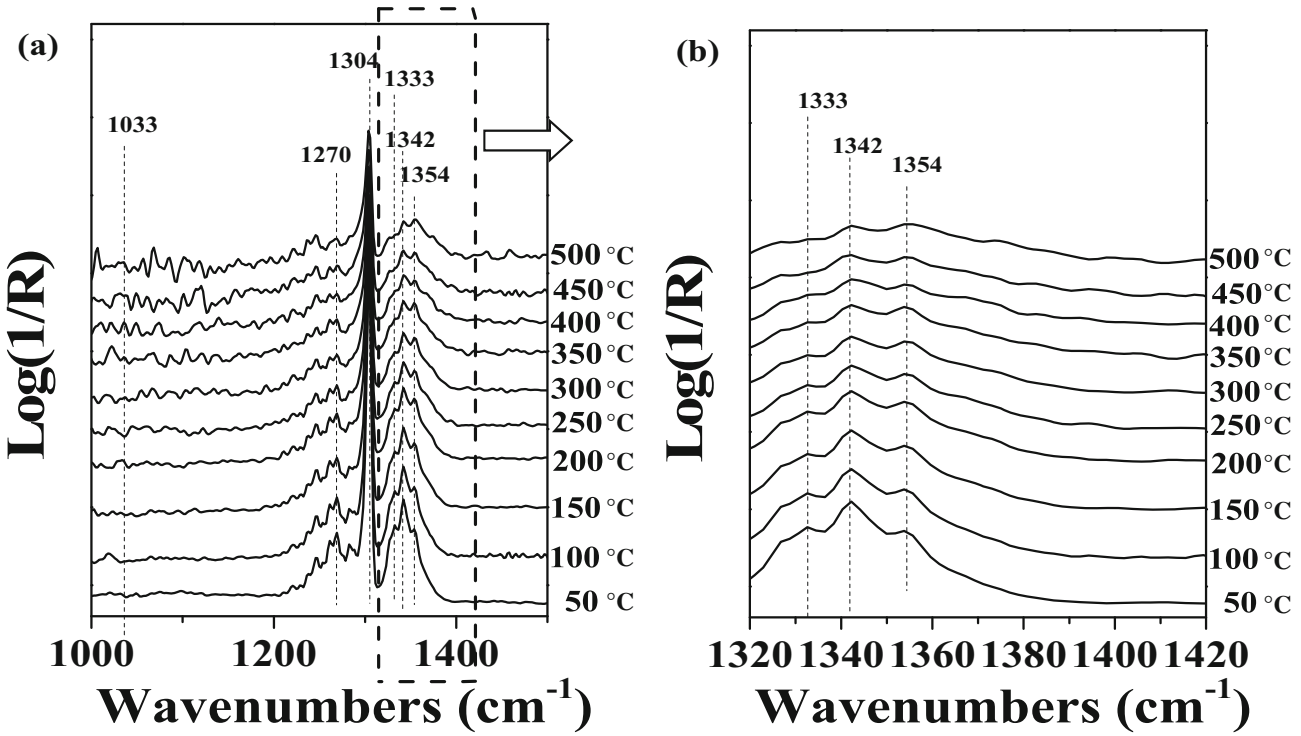

Figure 3. In situ DRIFTS results of Ni-Cu/MoO_x sample on cracking in the range (**a**) 1000–1500 cm^{-1}, (**b**) 1320–1420 cm^{-1}.

Table 4. The surface contents of Cu and Mo species on Ni-Cu/MoO_x by XPS results.

	Cu (%)			Mo (%)	
Samples	Cu^+	Cu^{2+}	Mo^{4+}	Mo^{5+}	Mo^{6+}
Sample 1	55	45	33	51	16
Sample 2	76	24	19	27	54
Sample 3	61	39	28	31	41

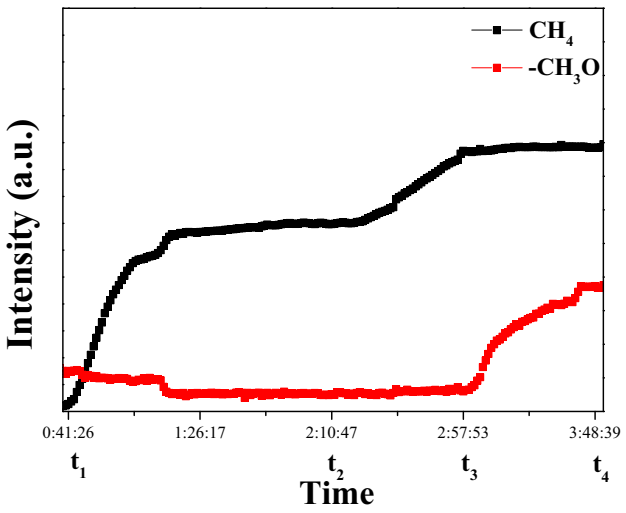

Figure 4. Mass spectrum of Ni-Cu/MoO_x sample on the whole cracking process. t_1: start cracking at 500 °C, t_2: start cooling at CH_4 atmosphere after cracking at 500 °C, t_3: the temperature was nearly at 350 °C, t_4: the temperature was nearly at 350 °C.

intensity of m/z = 31 (-CH_3O) for a while. During the cracking process at 500 °C (from t_1 to t_2, nearly 100 min), the peak of m/z = 31 (-CH_3O) showed very small intensity and varied little. When cooling was started (t_2), the intensity of m/z = 31 (-CH_3O) was still stable, and the intensity of m/z = 16 (CH_4) rose, which looked like CH_4 'desorption' on Ni-Cu/MoO_x. It could be speculated that CH_4 was more difficult to be cracked and adsorbed on Ni species of Ni-Cu/MoO_x at a lower temperature, so CH_4 cracking would be stopped gradually during the cooling process, which caused the amount of CH_4 accumulated. After that, owing to CH_4 cracking ceaselessly, it is very interesting to note that the intensity of m/z = 31(-CH_3O) rose a lot when cooling to nearly 350 °C (t_3), and then stopped rising at nearly 250 °C (t_4). Therefore, it could be indicated that alcohol (such as methanol or ethanol) precursor was generated in the cooling process.

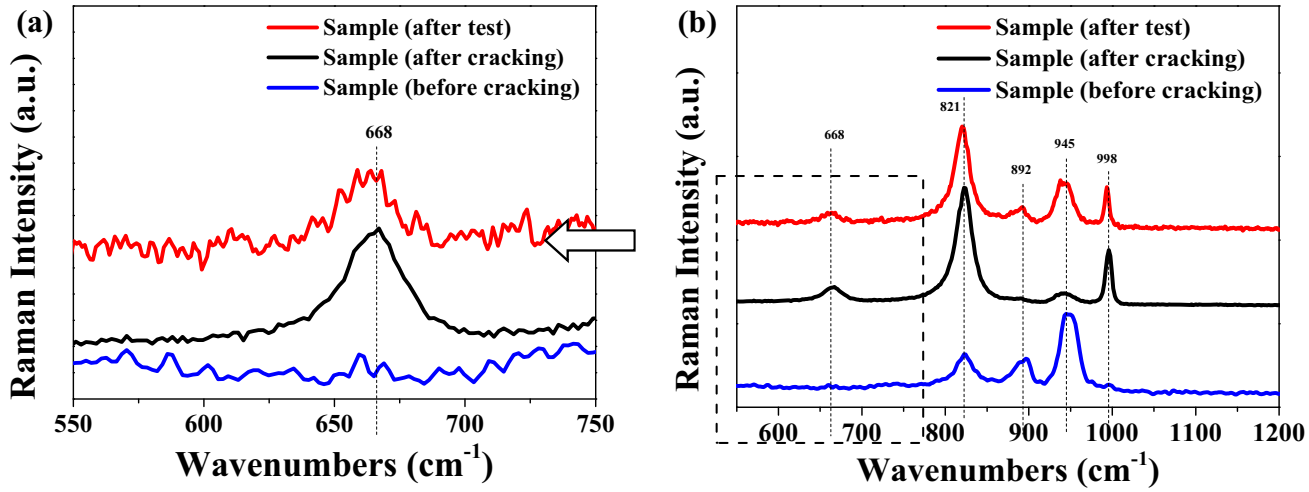

Figure 5. Raman spectra of Ni-Cu/MoO_x samples in the range (**a**) 550–750 cm^{-1}, (**b**) 550–1200 cm^{-1}.

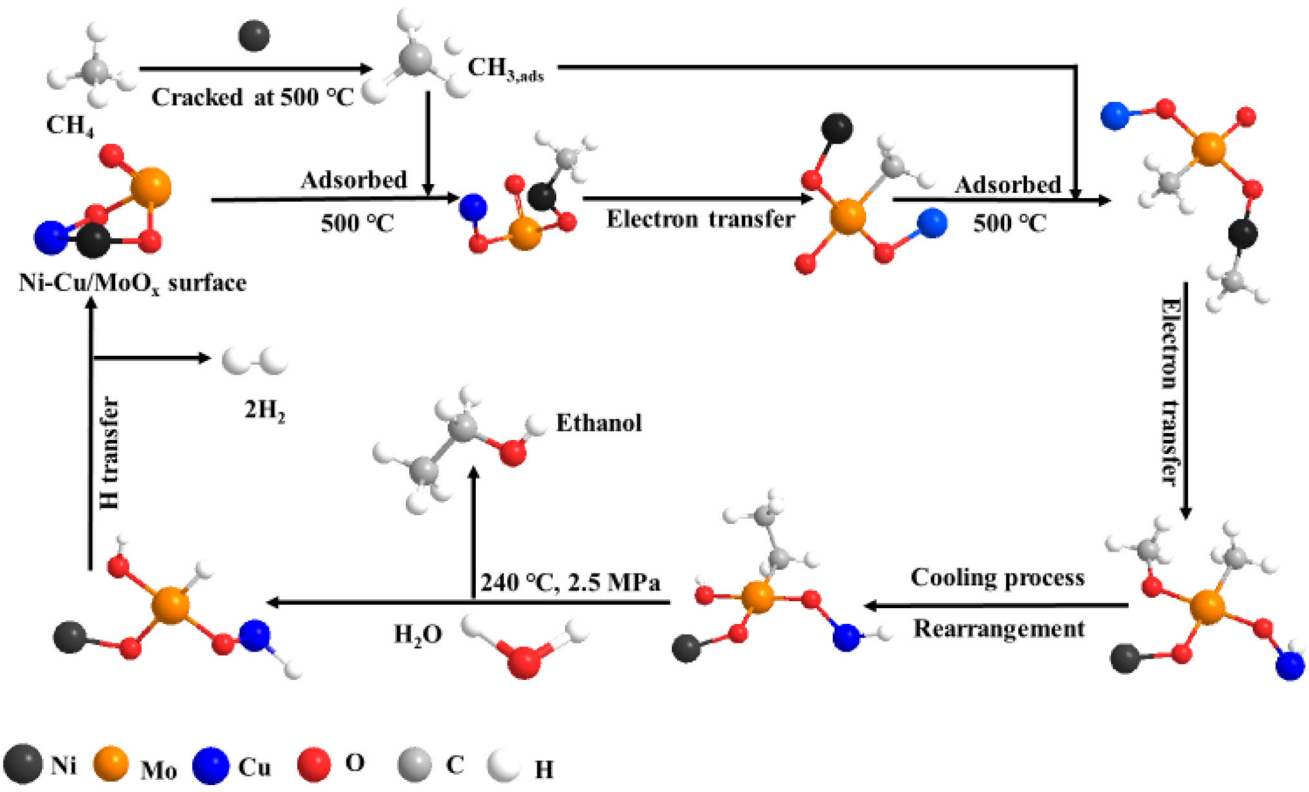

Figure 6. The tentatively schematic mechanism of the synthesis of ethanol from methane and water.

3.5 *Raman spectra*

The Raman spectra of Ni-Cu/MoO_x samples treated under three different conditions were obtained and shown in Figure 5. The Raman bands at 892 and 945 cm^{-1} were corresponding to Mo=O bond.[54,55] The appearance of the bands at 668, 821 and 998 cm^{-1}, could be associated with the symmetric and asymmetric O-Mo-O stretching vibrations, respectively.[56] It could be noticed that the intensity of Mo=O bond was high, and that of O-Mo-O bond was low relatively before cracking, and especially the intensity of the Raman band at 998 cm^{-1} was nearly none. However, after cracking, the intensity of O-Mo-O bond raised a lot, while that of Mo=O bond decreased much, and particularly the intensity of 892 cm^{-1}

almost vanished after cracking. Therefore, the phenomenon could indicate that some Mo=O bond could be converted to O-Mo-O bond owing to the interaction with CH_3 or H species which adsorbed on Ni species from CH_4 cracking. It could be seen that the intensity of Mo=O bond raised a little back after activity test, which could be associated with the effect that some precursors were taken away by adding water on Ni-Cu/MoO_x.

3.6 *Discussion*

According to the results above, a hypothetical mechanism tried to explain the production of ethanol from methane and water was proposed, as shown in Figure 6. Based on the *in situ* DRIFTS and XPS results, owing to the relatively short reduction time (1 h) and the formation of the special environment, no Ni^0 species was observed in the system. At first, $CH_{3,ads}$ would be adsorbed on Ni species which could result in the break of Ni-Cu bond. Then, due to the electron transfer, the $CH_{3,ads}$ would be taken away from Ni species and migrated onto the Mo species to break the Mo=O bond. Therefore, the oxide state of Mo species was changed from +5 to +6, while Cu species varied from +2 to +1. In the next step, another $CH_{3,ads}$ would be adsorbed on Ni species again, and H_{ads} would combine with the Cu species. Similarly, the $CH_{3,ads}$ would be also migrated onto the O species of new Mo-O bond with the help of Mo species again. At last, the added water could promote the rearrangement of this immediate, which caused the synthesis of ethanol, and H_2 would be obtained by the H transfer. Therefore, the reason for the necessary cracking process was the fact that more $CH_{3,ads}$ species could be attracted on Ni-Cu/MoO_x for further coupling.

4. Conclusions

Ni-Cu/MoO_x showed acceptable activity (18.5 μmol) for ethanol production from CH_4 and H_2O. The cracking process was very important because CH_3 species could be adsorbed and migrated on the surface of Ni-Cu/MoO_x. Ni species could help CH_4 crack to CH_3 species and adsorb on the surface, Mo species could provide CH_3 species with a reservoir for migrating and persistence, and Cu species could help adsorb H species for more convenience. Therefore, the rearrangement performed in the cooling process might be promoted by the synergetic effects of Ni, Cu and Mo species on Ni-Cu/MoO_x after cracking. These data provided a novel direction to the prospect of methane conversion to alcohol.

Supplementary Information (SI)

Figures S1–S5 and Tables S1–S2 are available as Supplementary Information at www.ias.ac.in/chemsci.

Acknowledgements

This work was financially supported by the National Key R&D Program of China (No. 2018YFB1501404) and 111 project (B17030). We thank Yunfei Tian of analytical & testing center of Sichuan University for XPS experiments.

References

1. de Angelis A 2012 Natural gas removal of hydrogen sulphide and mercaptans *Appl. Catal. B* **113–114** 37
2. Yang H 2014 China must continue the momentum of green law *Nature* **509** 535
3. Akri M, Pronier S, Chafik T, Achak O, Granger P, Simon P, et al. 2017 Development of nickel supported La and Ce-natural illite clay for autothermal dry reforming of methane: toward a better resistance to deactivation *Appl. Catal. B* **205** 519
4. Liu H, Li X and Hu Z 1996 Development of novel low temperature and low pressure ammonia synthesis catalyst *Appl. Catal. A* **142** 209
5. Lunsford J H 2000 Catalytic conversion of methane to more useful chemicals and fuels: a challenge for the 21st century *Catal. Today* **63** 165
6. Grundner S, Markovits M A, Li G, Tromp M, Pidko E A, Hensen E J, et al. 2015 Single-site trinuclear copper oxygen clusters in mordenite for selective conversion of methane to methanol *Nat. Commun.* **6** 7546
7. Ikuno T, Zheng J, Vjunov A, Sanchez-Sanchez M, Ortuno M A, Pahls D R, et al. 2017 Methane oxidation to methanol catalyzed by Cu-oxo clusters stabilized in NU-1000 metal-organic framework *J. Am. Chem. Soc.* **139** 10294
8. Narsimhan K, Iyoki K, Dinh K and Roman-Leshkov Y 2016 Catalytic oxidation of methane into methanol over copper-exchanged zeolites with oxygen at low temperature *ACS Cent. Sci.* **2** 424
9. Tomkins P, Mansouri A, Bozbag S E, Krumeich F, Park M B, Alayon E M, et al. 2016 Isothermal cyclic conversion of methane into methanol over copper-exchanged zeolite at low temperature *Angew. Chem. Int. Ed. Engl.* **55** 5467
10. Tomkins P, Ranocchiari M and van Bokhoven J A 2017 Direct conversion of methane to methanol under mild conditions over Cu-zeolites and beyond *Acc. Chem. Res.* **50** 418
11. Sushkevich V L, Palagin D, Ranocchiari M and van Bokhoven J A 2 017 Selective anaerobic oxidation of methane enables direct synthesis of methanol *Science* **356** 523

12. Sushkevich V L, Palagin D and van Bokhoven J A 2018 The effect of the active-site structure on the activity of copper mordenite in the aerobic and anaerobic conversion of methane into methanol *Angew. Chem. Int. Ed.* **57** 8906
13. Hammond C, Forde M M, Ab Rahim M H, Thetford A, He Q, Jenkins R L, et al. 2012 Direct catalytic conversion of methane to methanol in an aqueous medium by using copper-promoted Fe-ZSM-5 *Angew. Chem. Int. Ed.* **51** 5129
14. Zuo Z, Ramírez P J, Senanayake S D, Liu P and Rodriguez J A 2016 Low-temperature conversion of methane to methanol on CeO_x/Cu_2O catalysts: water controlled activation of the C-H bond *J. Am. Chem. Soc.* **138** 13810
15. Lustemberg P G, Palomino R M, Gutiérrez R A, Grinter D C, Vorokhta M, Liu Z, et al. 2018 Direct conversion of methane to methanol on Ni-ceria surfaces: metal-support interactions and water-enabled catalytic conversion by site blocking *J. Am. Chem. Soc.* **140** 7681
16. Yuan J, Zhang W, Li X and Yang J 2018 A high performance catalyst for methane conversion to methanol: graphene supported single atom Co *Chem. Commun.* **54** 2284
17. Williams C, Carter J H, Dummer N F, Chow Y K, Morgan D J, Yacob S, et al. 2018 Selective Oxidation of Methane to Methanol Using Supported AuPd Catalysts Prepared by Stabilizer-Free Sol-Immobilization *ACS Catal.* **8** 2567
18. Venkatathri N, Pillai V K, Rajini A, Nooka R M and Reddy I A K 2013 Structural and catalytic properties of a novel vanadium containing solid core mesoporous silica shell catalysts for gas phase oxidation reaction *J. Chem. Sci.* **125** 63
19. Polnišer R, Štolcová M, Hronec M and Mikula M 2011 Structure and reactivity of copper iron pyrophosphate catalysts for selective oxidation of methane to formaldehyde and methanol *Appl. Catal. A* **400** 122
20. Palkovits R, Antonietti M, Kuhn P, Thomas A and Schüth F 2009 Solid catalysts for the selective low-temperature oxidation of methane to methanol *Angew. Chem. Int. Ed.* **48** 6909
21. Pal S and Kundu T K 2013 DFT-based inhibitor and promoter selection criteria for pentagonal dodecahedron methane hydrate cage *J. Chem. Sci.* **125** 1259
22. Yao L, Shi J, Xu H, Shen W and Hu C 2016 Low-temperature CO_2 reforming of methane on Zr-promoted Ni/SiO_2 catalyst *Fuel Process. Technol.* **144** 1
23. Wang Y, Yao L, Wang Y, Wang S, Zhao Q, Mao D and Hu C 2018 Low-temperature catalytic CO_2 dry reforming of methane on $Ni\text{-}Si/ZrO_2$ catalyst *ACS Catal.* **8** 6495
24. Wang Y, Yao L, Wang S, Mao D and Hu C 2018 Low-temperature catalytic CO_2 dry reforming of methane on Ni-based catalysts: a review *Fuel Process. Technol.* **169** 199
25. Lin L, Zhou W, Gao R, Yao S, Zhang X, Xu W, et al. 2017 Low-temperature hydrogen production from water and methanol using Pt/α-MoC catalysts *Nature* **544** 80
26. Sutthiumporn K, Maneerung T, Kathiraser Y and Kawi S 2012 CO_2 dry-reforming of methane over $La_{0.8}Sr_{0.2}Ni_{0.8}M_{0.2}O_3$ perovskite (M = Bi, Co, Cr, Cu, Fe): Roles of lattice oxygen on C–H activation and carbon suppression *Int. J. Hydrogen. Energ.* **37** 11195
27. Oemar U, Hidajat K and Kawi S 2015 Pd–Ni catalyst over spherical nanostructured Y_2O_3 support for oxy-CO_2 reforming of methane: role of surface oxygen mobility *Int J. Hydrogen. Energ.* **40** 12227
28. Kim J H, Lee J, Kim J H, Hwang C C, Lee C and Park J Y 2015 Work function variation of MoS_2 atomic layers grown with chemical vapor deposition: The effects of thickness and the adsorption of water/oxygen molecules *Appl. Phys. Lett.* **106** 251606
29. Qiu H, Pan L, Yao Z, Li J, Shi Y and Wang X 2012 Electrical characterization of back-gated bi-layer MoS_2 field-effect transistors and the effect of ambient on their performances *Appl. Phys. Lett.* **100** 123104
30. Liu Y, Zhang H, Ouyang P, Chen W, Wang Y and Li Z 2014 High electrochemical performance and phase evolution of magnetron sputtered MoO_2 thin films with hierarchical structure for Li-ion battery electrodes *J. Mater. Chem. A* **2** 4714
31. Kosec T, Milošev I and Pihlar B 2007 Benzotriazole as an inhibitor of brass corrosion in chloride solution *Appl. Sur. Sci.* **253** 8863
32. Bin F, Wei X, Li B and Hui, 2015 K S Self-sustained combustion of carbon monoxide promoted by the Cu-Ce/ZSM-5 catalyst in CO/O_2 /N_2 atmosphere *Appl. Catal. B* **162** 282
33. Zhang M, Liu Z, Lin G and Zhang H 2013 Pd/CNT-promoted $CuZrO_2$/HZSM-5 hybrid catalysts for direct synthesis of DME from CO_2/H_2 *Appl. Catal. A* **451** 28
34. Khademi A, Azimirad R, Zavarian A A and Moshfegh A Z 2009 Growth and field emission study of molybdenum oxide nanostars *J. Phys. Chem. C* **113** 19298
35. Biradar A V, Sathe B R, Umbarkar S B and Dongare M K 2008 Selective cis-dihydroxylation of olefins using recyclable homogeneous molybdenum acetylide catalyst *J. Mol. Catal. A* **285** 111
36. Xiao S, Zhao X, Hu P, Chu Z, Huang C and Zhang L 2016 Highly photoluminescent molybdenum oxide quantum dots: one-pot synthesis and application in 2,4,6-trinitrotoluene determination *ACS Appl. Mater. Inter.* **8** 8184
37. Bykova M V, Ermakov D Y, Kaichev V V, Bulavchenko O A, Saraev A A, Yu Lebedev M and Yakovlev V A 2012 Ni-based sol–gel catalysts as promising systems for crude bio-oil upgrading: guaiacol hydrodeoxygenation study *Appl. Catal. B* **113–114** 296
38. Fang W, Paul S, Capron M, Dumeignil F and Jalowiecki-Duhamel L 2014 Hydrogen production from bioethanol catalyzed by $Ni_XMg_2AlO_Y$ ex-hydrotalcite catalysts *Appl. Catal. B* **152–153** 370
39. Kovács G J, Bertóti I and Radnóczi G 2008 X-ray photoelectron spectroscopic study of magnetron sputtered carbon–nickel composite films *Thin Solid Films* **516** 7942
40. Wang Z, Wang J, Li Z, Gong P, Ren J, Wang H, et al. 2012 Cooperatively exfoliated fluorinated graphene with full-color emission *RSC Adv.* **2** 11681
41. Cui Y, Du C, Gao Y, Yang J, Zhang L, Guan T, et al. 2016 Recovery Strategy and Mechanism of Aged Lithium Ion Batteries after Shallow Depth of Discharge at Elevated Temperature *ACS Appl. Mater. InterfacesMater. Interfaces* **8** 5234
42. Schuster M E, Hävecker M, Arrigo R, Blume R, Knauer M, Ivleva N P, et al. 2011 Surface sensitive study to

determine the reactivity of soot with the focus on the European emission standards IV and VI *J. Phys. Chem. A* **115** 2568
43. Zhang L, Wang J, Wang H, Xu Y, Wang Z, Li Z, et al. 2012 Preparation, mechanical and thermal properties of functionalized graphene/polyimide nanocomposites *Compos. Part A: Appl. Sci. Manufac.* **43** 1537
44. Kim H J, Lee K S, Won M S and Shim Y B 2008 Characterization of protein-attached conducting polymer monolayer *Langmuir* **24** 1087
45. Óvári L, Krick Calderon S, Lykhach Y, Libuda J, Erdőhelyi A, Papp C, et al. 2013 Near ambient pressure XPS investigation of the interaction of ethanol with Co/CeO_2(111) *J. Catal.* **307** 132
46. Kundu S, Wang Y, Xia W and Muhler M 2008 Thermal stability and reducibility of oxygen-containing functional groups on multiwalled carbon nanotube surfaces: a quantitative high-resolution XPS and TPD/ TPR study *J. Phys. Chem. C* **112** 16869
47. Venezia A M, Bertoncello R and Deganello G 1995 X-ray photoelectron spectroscopy investigation of pumice-supported nickel catalysts *Surf. Interface. Anal.* **23** 239
48. Sutthiumporn K and Kawi S 2011 Promotional effect of alkaline earth over Ni–La_2O_3 catalyst for CO_2 reforming of CH_4: role of surface oxygen species on H_2 production and carbon suppression *Int. J. Hydrogen. Energ.* **36** 14435
49. Wu T, Lin D, Wu Y, Zhou X, Yan Q, Weng W and Wan H 2007 In-Situ FT-IR investigation of partial oxidation of methane to syngas over Rh/SiO_2 catalyst *J. Nat. Gas. Chem.* **16** 316
50. Bader W, Mahieu E, Bovy B and Deneke T 2013 Evolution of methanol (CH_3OH) above the Jungfraujoch station (46.5° N): variability, seasonal modulation and long-term trend *J. Thorac. Cardiov. Sur.* **126** 836
51. Harman W D, Fairlie D P and Taube H 1986 Synthesis, characterization, and reactivity of the (.eta.2-acetone)pentaammineosmium(II) complex *J. Am. Chem. Soc.* **108** 8223
52. Pan Q, Peng J, Wang S and Wang S 2014 *In situ* FTIR spectroscopic study of the CO_2 methanation mechanism on Ni/$Ce_{0.5}Zr_{0.5}O_2$ *Catal. Sci. Technol.* **4** 502
53. Lavalley J C, Saussey J, Lamotte J, Breault R, Hindermann J P and Kiennemann A 1990 Infrared study of carbon monoxide hydrogenation over rhodium/ceria and rhodium/silica catalysts *J. Phys. Chem.* **94** 5941
54. Xie S, Chen K, Bell A T and Iglesia E 2000 Structural characterization of molybdenum oxide supported on zirconia *J. Phys. Chem. B* **104** 10059
55. Smaranda I, Baibarac M, Baltog I, Mevellec J Y and Lefrant S 2013 Spectroelectrochemical properties of the single walled carbon nanotubes functionalized with polydiphenylamine doped with heteropolyanions *J. Solid. State Chem.* **197** 352
56. Hirata T, Ishioka K and Kitajima M 1996 Raman spectra of MoO_3 implanted with protons *Appl. Phys. Lett.* **68** 458